



Separating the effects of changes in land cover and climate: a hydro-meteorological analysis of the past 60 yr in Saxony, Germany

M. Renner^{1,4}, K. Brust¹, K. Schwärzel^{2,*}, M. Volk³, and C. Bernhofer¹

¹Technische Universität Dresden, Faculty of Environmental Sciences, Institute of Hydrology and Meteorology, Chair of Meteorology, Tharandt, Germany

²Technische Universität Dresden, Faculty of Environmental Sciences, Institute of Soil Science and Site Ecology, Chair of Site Ecology and Plant Nutrition, Tharandt, Germany

³UFZ – Helmholtz Centre for Environmental Research, Department of Computational Landscape Ecology, Leipzig, Germany

⁴Max-Planck Institute for Biogeochemistry, Biospheric Theory and Modelling Group, Jena, Germany

* now at: United Nations University, Institute for Integrated Management of Material Fluxes and of Resources, Dresden, Germany

Correspondence to: M. Renner (mrenner@bgc-jena.mpg.de)

Received: 14 June 2013 – Published in Hydrol. Earth Syst. Sci. Discuss.: 2 July 2013

Revised: 11 October 2013 – Accepted: 18 December 2013 – Published: 31 January 2014

Abstract. Understanding and quantifying the impact of changes in climate and land use/land cover on water availability is a prerequisite to adapt water management; yet, it can be difficult to separate the effects of these different impacts. In this paper we illustrate a separation and attribution method based on a Budyko framework. We assume that evapotranspiration (E_T) is limited by the climatic forcing of precipitation (P) and evaporative demand (E_0), but modified by land-surface properties. Impacts of changes in climate (i.e., E_0/P) or land-surface changes on E_T alter the two dimensionless measures describing relative water (E_T/P) and energy partitioning (E_T/E_0), which allows us to separate and quantify these impacts. We use the separation method to quantify the role of environmental factors on E_T using 68 small to medium range river basins covering the greatest part of the German Federal State of Saxony within the period of 1950–2009. The region can be considered as a typical central European landscape with considerable anthropogenic impacts. In the long term, most basins are found to follow the Budyko curve which we interpret as a result of the strong interactions of climate, soils and vegetation. However, two groups of basins deviate. Agriculturally dominated basins at lower altitudes exceed the Budyko curve while a set of high altitude, forested basins fall well below. When visualizing the decadal dynamics on the relative partitioning of water and energy the impacts of climatic and land-surface changes

become apparent. After 1960 higher forested basins experienced large land-surface changes which show that the air pollution driven tree damages have led to a decline of annual E_T on the order of 38 %. In contrast, lower, agricultural dominated areas show no significant changes during that time. However, since the 1990s effective mitigation measures on industrial pollution have been established and the apparent brightening and regrowth has resulted in a significant increase of E_T across most basins. In conclusion, data on both, the water and the energy balance is necessary to understand how long-term climate and land cover control evapotranspiration and thus water availability. Further, the detected land-surface change impacts are consistent in space and time with independent forest damage data and thus confirm the validity of the separation approach.

1 Introduction

Evapotranspiration (E_T) is physically limited by the supply of both, water and energy (Budyko, 1974), while land-surface characteristics strongly modify the accessibility of water and absorbed energy for E_T . Hence the partitioning of water and energy at the land surface through actual evapotranspiration emerges from the interaction of various

land-surface processes under the atmospheric supply and demand for water.

One of the key questions for environmental sciences is how evapotranspiration E_T might vary under the pressure of environmental changes. Changes in the water partitioning into E_T and runoff are, for example, relevant for the management of water resources, agriculture and forestry, while changes in the energy partitioning may also affect regional climates (Milly and Dunne, 2001).

Thereby, it is important to highlight that potential changes in water–energy partitioning can be driven by global climate changes altering the supply of water and energy, or by local to regional scale land-surface changes (e.g., through human land use and management which alters land-surface processes). Both anthropogenic drivers of change are anticipated to increase in the future, both in magnitude and spatial extent. In order to sustain human well-being this requires careful planning and adaptation of environmental and natural resources management. For instance, specific land use and management changes might help to mitigate the impact of climatic changes on water resources. However, the development of successful mitigation strategies requires an improved knowledge on the sensitivity of the highly interlinked soil–vegetation–atmosphere system to external climatic changes as well as to internal changes of the land-surface properties (Dale, 1997). This task is challenging because (i) the boundary conditions are supposed to change, which questions the applicability of empirical parameterizations (Blöschl and Montanari, 2010; Merz et al., 2011); and (ii) climate and land-surface changes operate in different temporal and spatial scales but are likely to occur in parallel (Arnell, 2002; Pielke, 2005). Hence, there is considerable uncertainty to correctly attribute observed changes in E_T or runoff to climatic or land-surface changes (Walter et al., 2004; Milliman et al., 2008; Jones, 2011).

Here, we approach this problem by separating and quantifying the impacts of past climate and land-surface changes on the water–energy partitioning. We thereby propose a framework which is based on first-order principles of water and energy conservation valid for the scale of long-term annual averages. We propose that the impacts of climate and land-surface changes lead to distinctly different changes in the long-term annual average water–energy partitioning. Thereby, we extend previous work by Milne et al. (2002), Tomer and Schilling (2009) and Renner et al. (2012) who introduced the water–energy partitioning diagrams to separate both impacts.

The framework is applied on the catchment scale with E_T derived by closing the water balance. The combination of large meteorological and hydrological data archives enables the assessment of the role of the climatic drivers and potential land-surface changes on spatially integrated catchment E_T . We validate our findings through comparison with independent spatiotemporal data of land cover characteristics (forest damage data, land cover classification data from satellite

data) which in turn may help to distinguish climatic and direct land-surface impacts on vegetation.

For this purpose we use a comprehensive, long-term hydro-climate data set for the meso-scale region of the German Federal State of Saxony. The availability of runoff, precipitation and climate data allows us to assess the hydro-climatic changes of the past 60 yr (i.e., from 1950–2009). During this period the mountainous part of the region experienced a severe tree die-off due to heavy air pollution and subsequent tree damages. This die-off became known as the *Waldsterben* and was dominant from about 1970 to 1990. Since then, a period of forest recovery can be observed as a result of the industrial breakdown of eastern Europe and genuine efforts to reduce SO_2 emissions. This dramatic land-surface change, with effects on both transpiration and interception represents a challenging test case for the separation approaches. In relation to the land-surface changes, climatic changes, such as increases in annual average in temperature (Bernhofer et al., 2008) and changes in solar radiation, known as global dimming and brightening (Wild et al., 2005), have also been observed (Bernhofer et al., 2008; Ruckstuhl et al., 2008; Philipona et al., 2009).

The paper is structured as follows: in Sect. 2, we outline the separation method. The region, the hydro-climatic data set and the forest damage data are described in Sect. 3. In the results, Sect. 4, we first analyze the long-term average hydroclimatology of Saxony and then investigate the temporal changes and the role of climatic and land-surface changes. In Sect. 5 we then discuss the role of the apparent hydro-climatic controls under the impact of environmental pollution. Finally, conclusions are drawn in the last section.

2 Methods

2.1 Catchment water and energy balances

The core of the proposed data-analysis is to simultaneously analyze the water and energy balance of catchments. The simplified water balance equations for the long-term annual timescale reads

$$P = E_T + Q + \Delta S_w, \quad (1)$$

where we derive E_T through closing the long-term annual water balance by precipitation (P) minus runoff (Q) under the assumption of the catchment water storage change ($\Delta S_w = 0$). To highlight the role of energy exchange, the energy balance equation is written as water equivalents by dividing with the latent heat of vaporization (L):

$$R_n/L = E_T + H/L + \Delta S_e, \quad (2)$$

with net radiation (R_n), sensible heat (H) and an energy storage change term (ΔS_e). In the following we make use of the assumption that the available energy usually expressed

as R_n/L can be described by potential evapotranspiration E_0 (Choudhury, 1999; Arora, 2002).

A first-order limitation and control of E_T is described by the Budyko hypothesis: $E_{T,\max} = \min(E_0, P)$ leading to the water and the energy limit of E_T . Note, that the Budyko hypothesis is derived from steady-state conditions, which require the climate and land-surface conditions to be in equilibrium. Donohue et al. (2007) illustrate the role of non-stationary climatic or vegetation changes, while, for example, Istanbuluoglu et al. (2012) highlight the role of related changes in the storage term ΔS_w . Hence for applications of the Budyko framework it is necessary to check for non-stationary behavior as well as to use sufficiently long periods for averaging.

2.2 Separation of basin from climate change impacts on E_T

The separation of climate from land-surface changes can lead to valuable insights of past climatic and anthropogenic impacts, but it also may provide insight into how anticipated future changes may impact E_T . Here, we address simple, conceptual approaches to separate the effects of climate from land-surface changes. The idea of separating climate from land-surface changes is based on an approach suggested by Tomer and Schilling (2009) who analyzed changes in the relative partitioning of water and energy at the surface to separate climate and land-surface changes. Such hydroclimatic changes can be illustrated by the water–energy partitioning plot ($E_T/E_0 \sim E_T/P$ space). In the framework of Tomer and Schilling (2009) climate effects are assumed to alter both the water partitioning ratios and the energy partitioning ratios by the same magnitude but opposite signs, hence $\Delta(E_T/E_0) = -\Delta(E_T/P)$. Land-surface changes are assumed to shift $\Delta(E_T/E_0) = \Delta(E_T/P)$. Their framework implies (i) that climate changes are orthogonal to land-surface changes within the $E_T/E_0 \sim E_T/P$ space and (ii) the impacts of climate and land-surface changes are independent of the catchments climate (E_0/P) and catchment response (E_T). Renner et al. (2012) discuss their framework and Renner and Bernhofer (2012) show, for semi-arid basins in the US, that the aridity alters the change directions in the water–energy partitioning plot. Therefore, we will propose a modified concept of Tomer and Schilling (2009) which considers the effect of the climatic aridity on the separation of climate and land-surface changes.

Consider two dimensionless variables, which describe water partitioning as $q = E_T/P$ and energy partitioning $f = E_T/E_0$ as defined on an x - y axis in a cartesian coordinate system. Such a water–energy partitioning diagram is shown in Fig. 1 with the two states corresponding to different climatic (i.e., $\phi = E_0/P$) and hydrological conditions expressed as E_T . The line from origin where $E_T = 0$ through a respective point (q, f) corresponds to a fixed aridity index. Hence, we define a land-surface change by a change in E_T

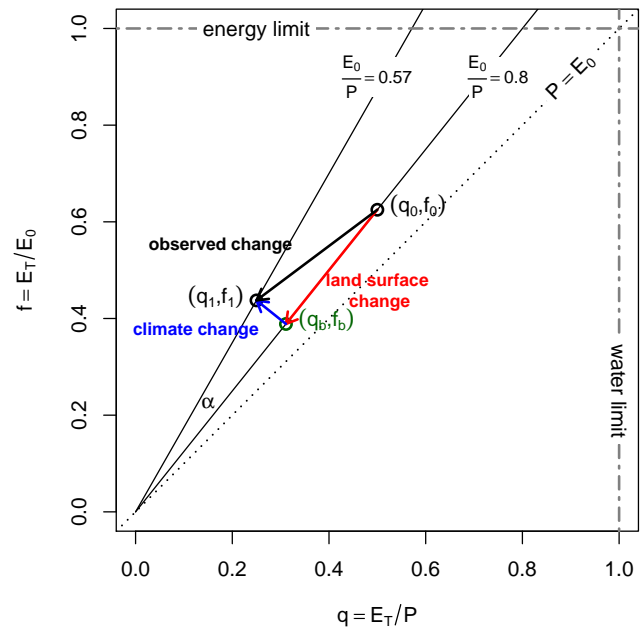


Fig. 1. Illustration of the separation of climate and land-surface changes in a q - f space diagram. The example shows two hydroclimatic states before (q_0, f_0) and after transition (q_1, f_1). The position of point (q_b, f_b) is determined by using the described geometric approach. The bold arrow lines depict the climatic and the land-surface components of this transition. For illustration we used case conditions of a base state: $P_0 = 1000$ mm, $E_{0,0} = 800$ mm, $E_{T,0} = 500$ mm and a state after hypothetical climatic and land-surface change with $P_1 = 1400$ mm, $E_{0,1} = 800$ mm, $E_{T,1} = 350$ mm. Thereby E_T decreased by 30 %.

but constant aridity. In the water–energy partitioning plot, the land-surface change direction is determined by the inverse of the aridity index P/E_0 . Next, we define climatic changes as changes in the aridity index which correspond to a change to a different ϕ line. Note, that this step is a major simplification in defining impacts of climatic changes and land-surface changes on E_T . Hence climatic changes are very strictly defined as changes in the average supply of water and energy. All other changes are referred to as land-surface changes, including direct human impacts such as land use and environmental pollution, as well as indirect effects due to greenhouse gas emissions and global warming. This also includes changes in the variability of climatic drivers.

Still, one problem remains, as we still need to define the direction of climatic changes within the water–energy diagram. Here we simply adopted the orthogonality assumption of Tomer and Schilling (2009) and assume that the climatic direction is perpendicular to the original ϕ related line. This implies that climatic impacts are independent of the catchment response (E_T). Hence, at any point along a constant aridity index (a line with the slope of P/E_0) the climate change direction simply is $-E_0/P$.

With the above assumptions we can derive the magnitude of both climate and land-surface related changes also for the case of simultaneous impacts. The derivation can be done in the cartesian space described by $q = E_T/P$ and $f = E_T/E_0$. Furthermore, we consider two observed points in this space (q_0, f_0) and (q_1, f_1) . The angle between both vectors can be described by the scalar product divided by the vector magnitudes to give

$$\sin(\alpha) = \frac{q_0 f_1 - q_1 f_0}{\sqrt{q_0^2 + f_0^2} \sqrt{q_1^2 + f_1^2}}. \quad (3)$$

Further the orthogonality assumption states that the climate change direction is perpendicular to the aridity index line on (q_0, f_0) . Hence we seek the coordinates of point (q_b, f_b) which is an intermediate state consisting of the land-surface change component and the climate change component of the observed changes. Again the sine of α can be related to the line segment of $((q_1, f_1); (q_b, f_b))$ and the magnitude of point (q_1, f_1) :

$$\sin(\alpha) = \frac{\sqrt{(q_b - q_1)^2 + (f_b - f_1)^2}}{\sqrt{q_1^2 + f_1^2}}. \quad (4)$$

Combining both Eqs. (3) and (4) and substituting $f_b = q_b f_0/q_0$ yields the x coordinates of point (q_b, f_b) :

$$q_b = \frac{f_0 f_1 q_0 + q_0^2 q_1}{f_0^2 + q_0^2}. \quad (5)$$

As it is defined that a land-surface change alters evapotranspiration at a constant aridity index, $E_{T,b}$ at point (q_b, f_b) can then be computed from q_b and the initial climatic conditions: $E_{T,b} = q_b P_0$.

The absolute differences of the observed evapotranspiration rates ($E_{T,0}$, $E_{T,1}$) to $E_{T,b}$ can then be used to determine the climatic ($\Delta E_{T,C}$) and land-surface ($\Delta E_{T,L}$) parts of change:

$$\Delta E_{T,L} = E_{T,b} - E_{T,0} \quad (6)$$

$$\Delta E_{T,C} = E_{T,1} - E_{T,b}. \quad (7)$$

Because this simple geometric approach is applied to discrete differences in a non-linear diagram, it remains somewhat arbitrary if we assume orthogonality at point (q_0, f_0) or point (q_1, f_1) . If the differences would be infinitesimally small than it would make no difference at which point we assume orthogonality. So, ideally we might use an integral of these small changes. For the geometrical approach this would yield a circle equation with origin at $(0, 0)$ and a radius defined by the point in the diagram. However, this step would complicate the approach and the differences are small compared to the overall changes and the detection thereof (changes in E_T , P , E_0).

The proposed method can in principle be applied to any reasonable hydro-climatic state, however, when E_T is close to a limitation ($E_T/P \rightarrow 1$ or $E_T/E_0 \rightarrow 1$) then the orthogonality assumption violates the first principles of mass and energy conservation. Hence, accounting for water limitation or energy limitation implies that the catchment response E_T must also be taken into account. Yang et al. (2008) show that this yields the Mezentsev (1955) or Choudhury (1999) parametric Budyko function. The Choudhury equation only yields an orthogonal response of climate to land-surface change, when its parameter is set to $n = 2$ which is identical to the classic Pike (1964) equation. Other classic Budyko curves (Schreiber, 1904; Ol'Dekop, 1911; Budyko, 1948) are similar but yield not exactly orthogonal responses of E_T to climate. Also note that the climate elasticity studies of Dooge (1992) and Arora (2002) use the slope at a given aridity index of these classic Budyko functions. Hence, these studies derive the climatic sensitivity also independently of the actual catchment response. By employing a parametric Budyko curve such as the Choudhury (1999) or the Fu (1981) curve, the effect of the catchment response can be taken into account (Yang et al., 2008; Roderick and Farquhar, 2011). At higher n (or E_T) the Choudhury curve is more bent towards the limits, whereas at $n < 1$ the curve bends towards ($E_T/P \rightarrow 0$ or $E_T/E_0 \rightarrow 0$). To our knowledge, however, there exists no empirical evidence of these mathematically derived sensitivities of E_T to changes in climate, when n is smaller than 1.

Similar studies on separating climate from land-surface changes directly employ a Budyko type of function to predict the climate related change in E_T and attribute the difference to a land-surface impact (Wang and Hejazi, 2011; Jaramillo et al., 2013). In contrast the presented geometrical separation method has the benefit that it does not require a Budyko type of function for application.

3 Study area and database

In the following a brief overview of the study areas is provided, followed by a description of the data base.

3.1 Study area

The study area, the Federal State of Saxony, is located in the eastern part of Germany and covers an area of about 18 500 km². The topography of the region is characterized by lower elevations of 100 m in the northern parts to higher elevations of up to 1200 m in the southwest (Ore Mountains, "Erzgebirge") see also Fig. 2. The temperate warm and humid climate with a distinct seasonal course in temperature is mainly controlled by the orography and a moderate west to east transition of maritime to continental climatic conditions.

The mountainous parts in the south receive most precipitation and thus play an important role for water resources. Due

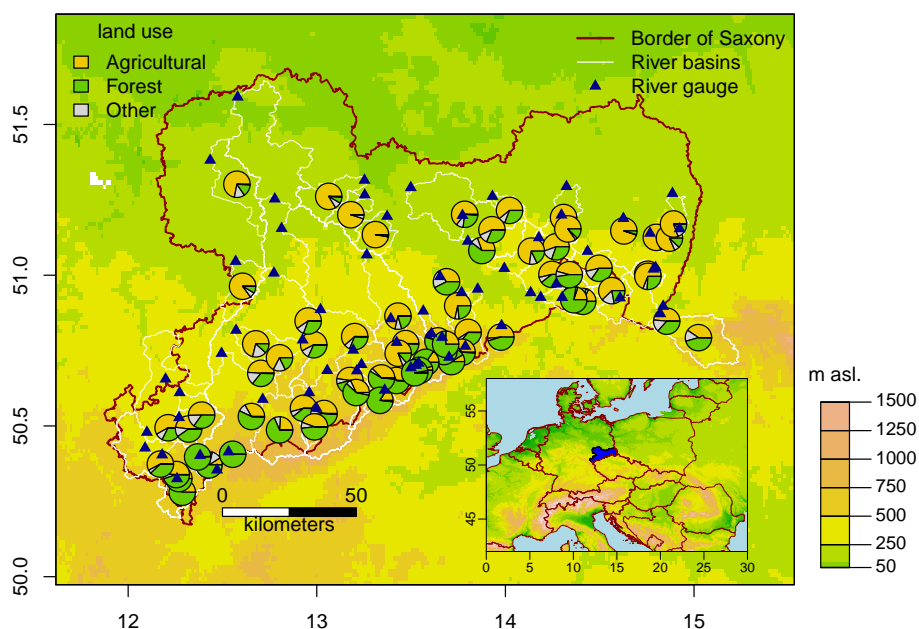


Fig. 2. Topography of the Federal State of Saxony/Germany, river basin divides, river gauging stations and dominant land use. The blue polygon in the inset shows the border of Saxony within central Europe.

to the colder climate, mountainous topography and less fertile soils, these parts are mainly covered by forests, whereas the lower regions are agriculturally dominated. The ratio of forest to agricultural land use is reported on a catchment basis in Fig. 2.

Land use and land cover in eastern Germany have been affected by changes in agricultural policies after World War II (Baessler and Klotz, 2006). Especially during the “collectivization” period (1952–1968) small farms were pooled to form large agricultural producers’ cooperatives (“LPG”). However, 1990 marked another major turning point in agricultural policy, with the privatization of agricultural land following the political changes in the former East Germany (Eckart and Wollkopf, 1994). The proportion of agricultural land has decreased from 57 % in 1992 to presently 55 % of the area of Saxony (StaLa, 2012), of which around 23.7 % is used as pasture. Forests cover at present in total 27.2 % of the state’s area (in comparison to around 26 % in 1992). Forest vegetation was heavily impacted by air pollution, with subsequent tree die-off since the 1960s and with major clear cuts in the 1980s (Šrámek et al., 2008) at the mountain ridge in southern Saxony. Such dramatic changes in vegetation cover may have also influenced hydrologic processes. Between 1991 and 2012, the proportion of damaged forest decreased from 27 to 16 % of the total forested area (SMUL, 2006). Urban and infrastructure areas have increased from around 10 % in 1992 to 12.6 %.

3.2 Runoff data

The Federal State of Saxony operates a dense network of hydrological gauging stations with a rich set of locations having long observation histories. The network density further increased in the 1960s. We have chosen river gauge stations, which almost fully cover the period 1960–2000. The daily discharge data have been converted to monthly runoff depth (mm month^{-1}) using the respective catchment area. Then runoff data were subjected to a homogenization test procedure; first on the runoff ratio (Q/P), and second using the weighted mean reference series of neighboring catchments. We also removed basins with large dams, compared to basin size. The remaining 68 stations cover large parts of Saxony, with catchment areas ranging from 5 to 6171 km^2 . Most stations are within the Mulde River basin (23) or are located at the tributaries of the Upper Elbe (18). Note, that some of the stations are directly connected and are not independent. Detailed information can be found in Table S1 in the Supplement. The locations of the gauging stations and catchment areas can be found on the map provided in Fig. 2. All further procedures are based on annual values using the definition of hydrological years (1 November to 31 October).

3.3 Precipitation data

The precipitation data collection network in Saxony and neighboring states is also quite dense. We selected the spatial interpolation method of Renner and Bernhofer (2011) and chose the geographical domain (11.5–16° E, 50–52° N). The daily station data was accumulated to annual values for

interpolation. To account for the height dependency, a linear height relationship was established using a robust median based regression (Theil, 1950). Then the residuals have been interpolated onto an aggregated SRTM grid (Jarvis et al., 2008) of 1500 m raster size using an automatic ordinary kriging (OK) procedure (Hiemstra et al., 2009). Annual basin average precipitation is then computed by the weighted average of the respective grid cells. The method of height regression and OK of the residuals was chosen, as this method showed to have the lowest root mean square errors (RMSE) among other methods, in a cross-validation based on annual station data sets (not shown).

Besides the spatial interpolation uncertainty, two other sources of uncertainty dominate the annual precipitation estimates time series. First, there is a precipitation bias. To account for this effect, we performed a precipitation correction of the annual precipitation sums using the Richter (1995) scheme which is largely based on rain gauge sheltering factors and altitude. The bias correction only led to a shift in precipitation related data, but did not change the overall features. For further analysis, we used the uncorrected values. A second uncertainty is the varying number of available stations in the domain. To account for this problem, three different sets of interpolated precipitation time series have been produced, (a) fixed net of stations covering the full period and (b) all available stations at a time. We assessed the differences and opted for a compromise between (a) and (b) with stations covering large parts of the core period 1960–2000.

3.4 Potential evaporation

To describe the evaporative demand we employ a parametric potential evapotranspiration scheme. This has the advantage of the use of standard meteorological data for estimation. Donohue et al. (2010) have shown that trends in various input data can lead to different trends in E_0 depending on which scheme and thus input variables have been used. Thereby the physically based Penman scheme yielded the most reasonable magnitudes and trends (Donohue et al., 2010).

For annual E_0 estimates we make use of the FAO (Food and Agricultural Organization) grass reference evapotranspiration method (Allen et al., 1994). This simplification of the Penman–Monteith equations is widely used as it provides many alternative ways to use available input data. Here we first compiled monthly averages of daily station data of temperature (mean, minimum, maximum), sun shine duration, relative humidity and wind speed data. The locations of the climate stations used are shown as dots in Fig. 3b. The aggregated annual totals were then spatially interpolated with an automatic universal kriging procedure with station elevation as local trend variable (Hiemstra et al., 2009).

Table 1. Forest damage classification.

Condition	[%] damaged trees per stand
no damage	0
Little damage	> 5
Moderate damage	6–30
Heavy damage	31–70
Dead	> 71

3.5 Land cover and vegetation data

The characterization and quantification of hydrological effects of land-surface changes such as land use change or forest damage would ideally require several temporal snapshots over the study area. Here, we use the satellite based Corine land cover data set and forest damage data to assess forest health over time.

3.5.1 Corine land cover classification

For the assessment of dominant land cover types in the analyzed catchments, we used the Corine Land Cover raster data set of the year 2000 available from the European Environment Agency (EEA). The data show different levels of land cover classes and aggregated types of forested and near natural vegetation classes are combined as “forest”, whereas all agriculturally and grass lands are merged as class “agricultural”.

To compute the area of damaged forest within a catchment, we used the Corine land cover class transitional scrub forest (324). This land cover class includes areas of damaged forests (cf. Bossard et al., 2000). A visual comparison showed good agreement of these maps with the forest damage maps in Fig. 7d.

3.5.2 Forest damage data

Here, we use maps of ground-based canopy damage data available for the years 1960, 1970, 1980 and 1990 which rely on the measurement standards defined in the former German Democratic Republic (Forstprojektion, 1970). The maps use a damage classification which is shown in Table 1. This measurement standard relies on needle and leaf losses in the canopy (SMUL, 2006). Although in recent years more comprehensive measures have been used to describe the stand productivity (Zirlewagen, 2004), these more complex data are not easy to compare with the former standards.

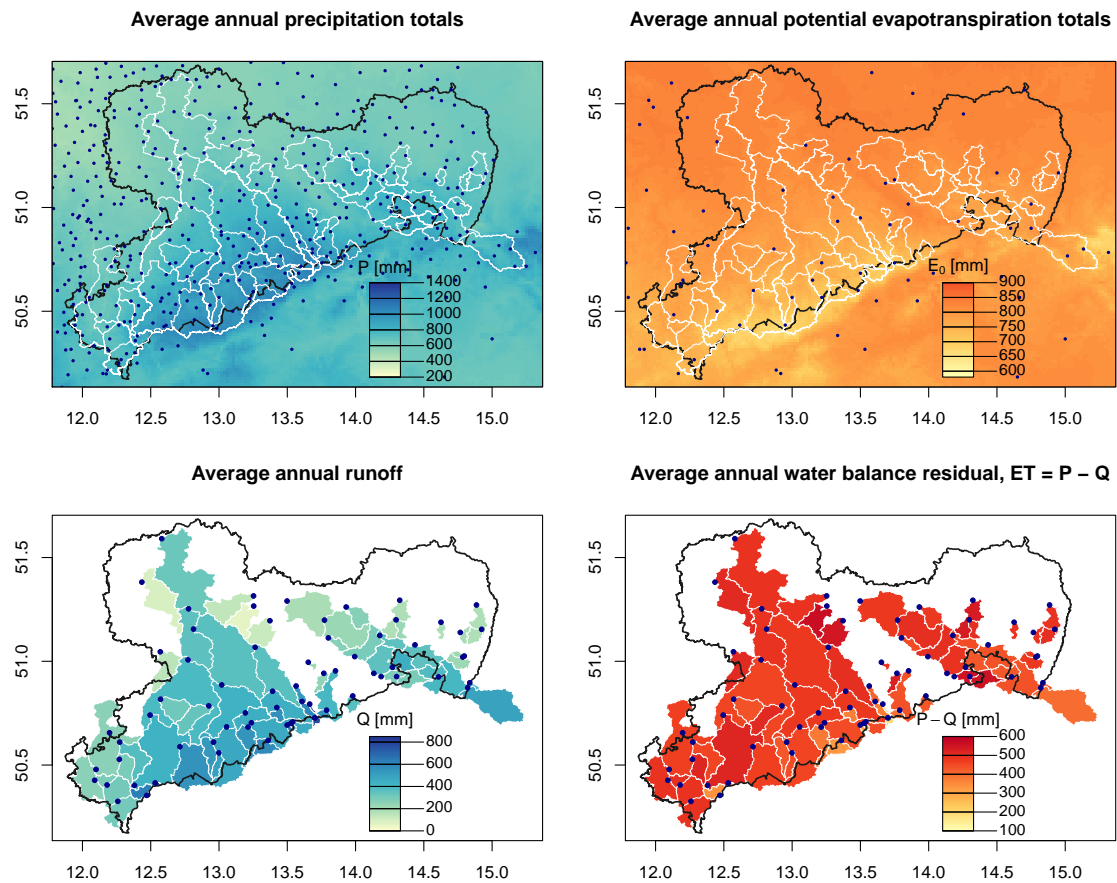


Fig. 3. Maps of long-term (1950–2009) annual average values for (a) precipitation, (b) annual potential evapotranspiration (FAO-Reference, Allen et al., 1994), (c) annual runoff and (d) the residual water budgets ($E_T = P - Q$). Observation stations are depicted as dots. The maps of annual average of precipitation P and the FAO reference potential evapotranspiration E_0 have been derived by averaging the individual annual raster maps used to calculate the basin averages. Note, that each graph has its own color scale.

4 Results

4.1 Hydroclimatology of Saxony

In this section the long-term average (1950–2009) hydroclimatology of Saxony is illustrated based on the established data set.

Annual average observed station precipitation within the study area ranges between 425 and 1340 mm yr⁻¹ and has a distinct north to south increasing gradient which is linked to topography. Another, although weaker gradient is induced by the transition of maritime to continental climate which results in decreased precipitation from west to east (Fig. 3a). The calculated FAO reference potential evapotranspiration E_0 ranges between 554 and 881 mm yr⁻¹ and is negatively correlated with precipitation showing a decrease with higher elevation (see Fig. 3b). Runoff largely follows the precipitation gradients showing the lowest annual values in the north (minimum 63 mm yr⁻¹) and increasing with height in the south (maximum 824 mm yr⁻¹). As visible from Fig. 3c, the runoff pattern is dominated by the Mulde River basin which

receives a large share of its water from the headwater catchments in the Ore Mountains. By closing the water balance we estimate actual catchment evapotranspiration (Fig. 3d). The lowest values of annual E_T are found in the high headwater basins (minimum 188 mm yr⁻¹). The pattern of the higher E_T (> 500 mm yr⁻¹) is more complex. These patterns are predominantly found in areas of large potential evapotranspiration (north and east), but also in areas with high annual precipitation and relatively gentle slopes such as in the southwestern part. All long-term average data can also be found in Table S1 (Supplement).

A simple correlation analysis (cf. Table 2) of the basin averages of altitude, forest cover, groundwater influence, climate, water and energy partitioning reveals strong links of hydrology, atmospheric forcing and landscape characteristics. This suggests strong interactions of climate, land use and water–energy partitioning induced by the topographical gradients.

Table 2. Altitude effects on climate, water–energy balance, groundwater influence (estimated as one year lag cross-correlation coefficient of precipitation and runoff, $\rho_{P_{t-1};Q_t}$) and percentage of forest cover. Reported are Pearson correlation coefficients for the long-term averages of all basins. All relations are significant with $p < 0.001$.

	Altitude	ϕ	P	E_0	E_T/P	E_T/E_0	$\rho_{P_{t-1};Q_t}$
Altitude							
ϕ	−0.93						
P	0.93	−0.99					
E_0	−0.98	0.90	−0.89				
E_T/P	−0.89	0.91	−0.91	0.86			
E_T/E_0	−0.65	0.58	−0.61	0.61	0.86		
$\rho_{P_{t-1};Q_t}$	−0.72	0.62	−0.67	0.68	0.70	0.65	
Forest cover	0.78	−0.75	0.76	−0.78	−0.77	−0.62	−0.57

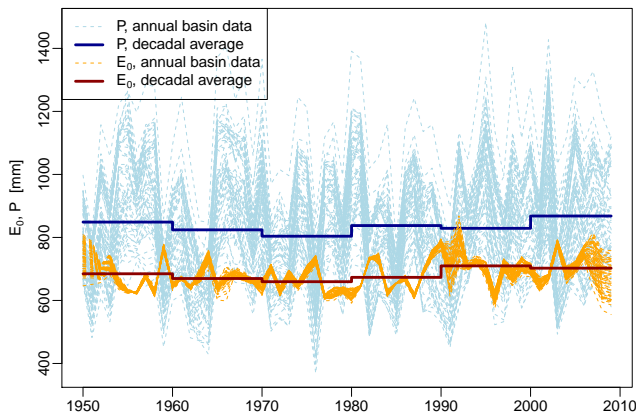


Fig. 4. Time series of annual P and E_0 for all basins and the all basin decadal averages.

Variability of annual precipitation and potential evapotranspiration

To get an overview of the temporal dynamics of P and E_0 we plot time series of both variables for all catchments in Fig. 4. For precipitation, a large temporal variability can be observed for all basins, but with considerable spatial coherence. Because of the large natural variability there are hardly any significant signals of structural changes in basin precipitation. We only find a gentle decrease after 1960 and an increase since about the 1990s.

We estimated the evaporative demand by using the FAO reference potential evapotranspiration. This series shows less year to year variability and much stronger spatial coherence than precipitation (see Fig. 4). From the data, we observe a period of lower average E_0 between 1960 and 1990 with a significant increase after 1990. This structural change is also found in observations of sunshine duration (not shown). With regard to the aridity index $\Phi = E_0/P$ the observed trend changes in E_0 are, however, much smaller than the variability of P and thus not detectable in a Φ series.

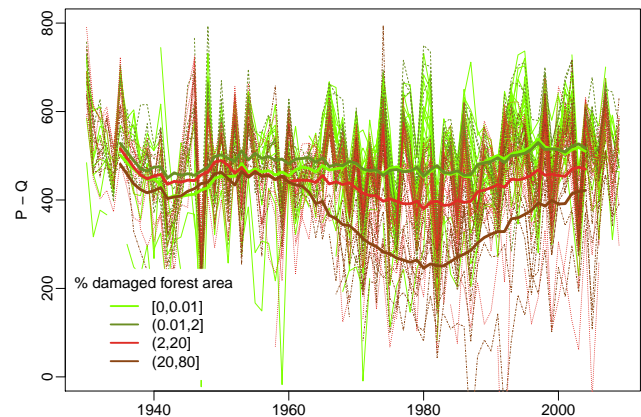


Fig. 5. Time series of $P - Q$ in the period 1930–2009, where runoff data was available. The thin lines show annual data of all catchments. In bold are 11 yr moving averages of certain groups of basins. The grouping and coloring follows the range of damaged forest area per basin using the Corine 1990 class 324 (transitional scrub forest). Note that for the 11 yr averages (bold lines) all available data of each group have been used.

4.2 Variability of basin evapotranspiration

By taking the annual water budget residual $P - Q$, we analyze the interannual variability in basin scale E_T , however, including the unknown influence of past water storage changes (ΔS_w). The annual $P - Q$ dynamics are plotted in Fig. 5. For the plot all basin data within the period 1930–2009 are used. The interannual dynamics are consistent over the basins analyzed with significant influence of the interannual variability in annual precipitation and potential evapotranspiration. In the long run, the average water storage term can be assumed to diminish, hence we smooth the data using a 11 yr moving average in Fig. 5. To investigate if forest damage may have affected basin scale E_T , we classified the basins into 4 categories according to the relative basin area where forest damage has been detected. To estimate this effect we use the transitional scrub forest class in the Corine data set of the year 1990. Although this represents a temporal

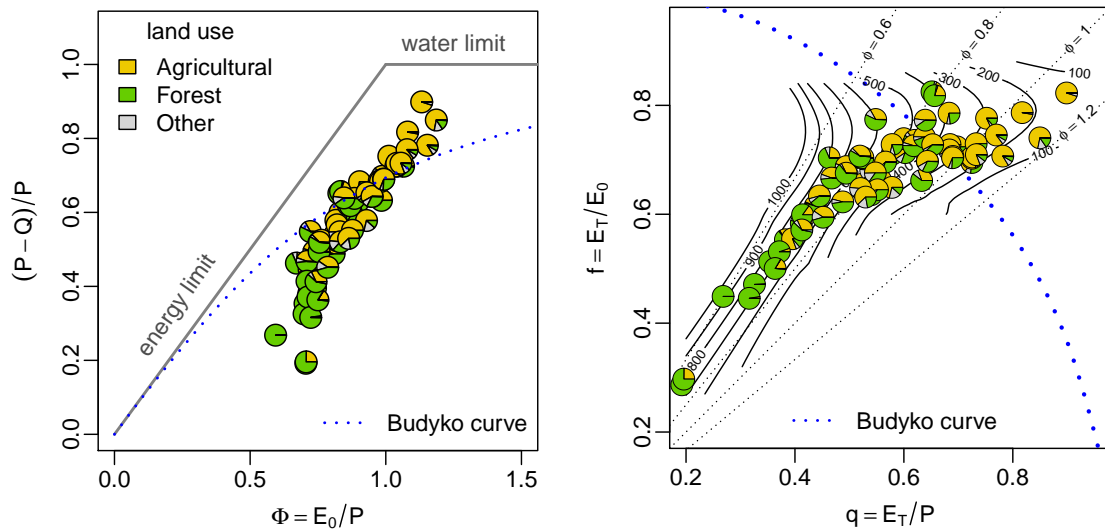


Fig. 6. Long-term (1950–2009) basin climate and water balance plots showing the Budyko space plot in the left and the water–energy partitioning plot in the right panel. The pie-charts show the areal percentage of land use of each basin. In the right panel, the average basin elevation is used to predict the contour lines using LOESS regression. This demonstrates the general height dependency of the basins climate. Further, the transition from wet basins with high runoff ratio to lower values is also reflected by land use.

snapshot without detailed knowledge of the magnitude and start of the forest damage it clearly indicates an area which has been significantly changed in the past. Using this classification we found that 38 % of the basins have no damage (< 0.01 %), 21 % have minor affected areas (0.01–2 %), 31 % have considerable damaged areas (2–20 %), and 10 % of the basins have damaged areas larger than 20 %. We used this classification to compute the group moving averages of $P - Q$. For the first period from 1930 to about 1960, no large deviations between these groups can be observed although larger decadal scale variability was evident. After 1960 the series start to deviate strongly with the damaged areas showing a significant decline in $P - Q$. Since the 1980s the trend has reversed and there is a general increase in all groups. However, the group with the highest proportion of damaged forest shows the strongest increases towards the 1990s and 2000, with smaller deviations between these groups. The damaged group of basins show similar high values to those observed in the 1950s, whereas the other basins show even higher $P - Q$ values. Already from Fig. 5 it can be deduced that forest damage can explain the larger deviations in basin scale evapotranspiration. Further, climatic variability which is rather coherent over the area of Saxony, shows a distinct effect, although of smaller magnitude.

4.3 Separation of climate and land-surface impacts on E_T

Having detected the influence of both, land-surface and climatic changes on basin scale E_T , we now employ the separation method illustrated in Sect. 2 to attribute the observed variability of E_T to the variability in the aridity of climate

and the land-surface variability. We first illustrate the separation framework in a cross-basin analysis of long-term annual average conditions and then apply the separation using the water–energy partitioning diagrams on the decadal timescale. Finally, we test the attribution approach by using the independent forest damage data.

4.3.1 Cross-basin analysis of climate and land-surface impacts

To illustrate the influence of the climate on long-term average evapotranspiration we use the classical Budyko curve which is shown in Fig. 6. The evaporation ratio ($(P - Q)/P$) of the various catchments increases with increasing aridity index ($\Phi = E_0/P$), but there is considerable deviation from the theoretical Budyko curve. The reasons for that could be a bias in E_0 and P basin estimates. However, such a bias would shift the whole group of basins to the left or right, without changing the apparent slope. By adding land use information (derived from Corine and aggregated to forest and agricultural land cover ratios per basin), it seems that the dominant land use caused the deviation from the Budyko curve. Thus, basins with dominant agricultural land use are well above and a set of forested basin are found well below the Budyko curve. However, a large part of basins, mainly with mixed type of vegetation, is still well represented by the Budyko curve.

Impacts of climate and land-surface conditions can be better represented by a water–energy partitioning plot introduced with Fig. 1 which is populated with the same data as in Fig. 6. In Fig. 6, values in the lower left corner indicate low E_T in relation to precipitation and E_0 , while at the opposite

corner most of the water and the energy is used for evapotranspiration. To recap, the direction of change along an aridity line reveals dominant land-surface change impacts, whereas if the direction of change is perpendicular to an aridity line, the climatic change impacts are dominant. Besides land use information, we also depict the altitude dependency as contour lines within the water–energy partitioning plot. Note, that these contour lines follow approximately lines of constant aridity (dotted lines). That means the higher the altitude the more humid the climatic conditions. From the cross-basin correlation analysis we found that basin altitude and the aridity index are strongly, but negatively correlated ($R = -0.93$). Although some of the variability in water–energy partitioning is explained by the aridity of the climate, many values in Fig. 6 stretch along these lines of constant aridity. This indicates that the largest variability within the set of basins is due to the variability of water–energy partitioning, rather than climate forcing. This variability is linked to land cover, as indicated by the pie charts. Hence, basins with a higher proportion of forests are located in the lower left corner, whereas the agricultural dominated basins largely are found in the upper right corner of the water–energy partitioning plot. These patterns thus support our assumption of different climate and land-surface change directions which were elaborated in Sect. 2.

4.3.2 Decadal dynamics of water–energy partitioning

With Fig. 1 we illustrate that the direction of observed changes in the long-term average water–energy partitioning reveals the dominant impacts on hydroclimatology. We make use of this simple detection approach and plot the decadal averages in the water–energy partition diagrams in Fig. 7, where we assume that ΔS_w is negligible. We visualize the change direction from one decade to the next with an arrow pointing to the average value of the next decade. Although the resulting trajectories are mostly coherent, we use a two sample Hotellings T2 test (Todorov and Filzmoser, 2009) with a significance level of $\alpha = 0.1$ to denote any changes larger than the interannual variability caused by water storage changes. In the lower right of each panel a map of forest damage in Saxony is drawn. Additionally, we show the trajectories using the river gauge location as origin of the respective arrow. This then helps to determine the locations and directions of dominant hydro-climatic changes and their relation to forest damage inventory data.

Looking at the decade 1950–1959 in Fig. 7a, we find the hydro-climatic conditions of the basins to be generally close, although not all basins were gaged at that time. The trajectories towards the 1960s are rather short and do not reveal statistically significant changes. Some forest damages are located in smaller areas in the Ore Mountains along the southern border of Saxony and in the Leipzig lowlands in the northwest. Note, that the northwest and the northeast of Saxony have been highly impacted by open pit mining for

lignite (Grünewald, 2001). Due to massive hydraulic engineering, many river gauge records are very difficult to interpret in terms of evaporation changes and thus have been excluded from this analysis. Forest damages continued increasing during the 1970s and the trajectories showing the transition from the 1960s to the 1970s reveal a dominant land-surface change pattern with some significant changes mainly in the Ore Mountains and Upper Lusatia in the east (Fig. 7b). This pattern continues when we look at Fig. 7c with even more forests damaged and to a greater extent. Figure 7d shows a consistent and large upward trend in land-surface related E_T change along the Ore Mountains with the most significant changes for the whole period. This land-surface related impact is accompanied with a change in the climatic forcing, namely the increase in E_0 (see Fig. 4), which is more apparent in basins with higher water–energy partitioning ratios. In this case the higher atmospheric demand for water led to an increase of the water partitioning ratio (see Fig. 7d). At that time, reported forest damage was a major environmental issue affecting most of the forests in Saxony. Since 1990 also high-resolution remote sensing land cover classification can be used to identify forest damage on a transnational scale, which we show as blue raster cells at a 100 m spatial resolution in the inset map. This shows hot spots of forest damages in the Ore Mountains, the Jizera Mountains and the North Bohemian Basin, also impacted by lignite mining and related emissions. The water–energy plot in Fig. 7e shows continuous increases in E_T with dominant land-surface impacts which are accompanied by a significant increase in precipitation (Fig. 4) when considering the changes from the 1990s to the first decade in 2000. In that case, increasing precipitation values with almost constant E_0 lead mainly to an increase of the energy partitioning ratio, indicating a contribution of climate variability. The comparison of the first decade (Fig. 7a) with the last decade (Fig. 7f) of the analysis reveals similar hydro-climatic states. This highlights a hydrological recovery of most of the forested basins and a dominance of the climatic aridity in controlling the variability of E_T in these decades.

4.3.3 Quantification of impacts

Using the geometric separation approach illustrated in Sect. 2.2, we computed the land-surface and climate related contribution of the observed E_T anomalies. As reference period for computing the anomalies we choose the 2000–2009 decade, because of data availability and the side effect of having the highest E_T values of the study period (Fig. 5). The observed and attributed anomalies for all basins and all decades are shown in the image plots in Fig. S1 in the Supplement. The results show that the observed total anomalies generally increase with basin altitude and can be as large as -233 mm yr^{-1} . The climate related anomalies are consistent across all basins, however, on a smaller magnitude. The largest climatic anomalies with respect to the 2000s are

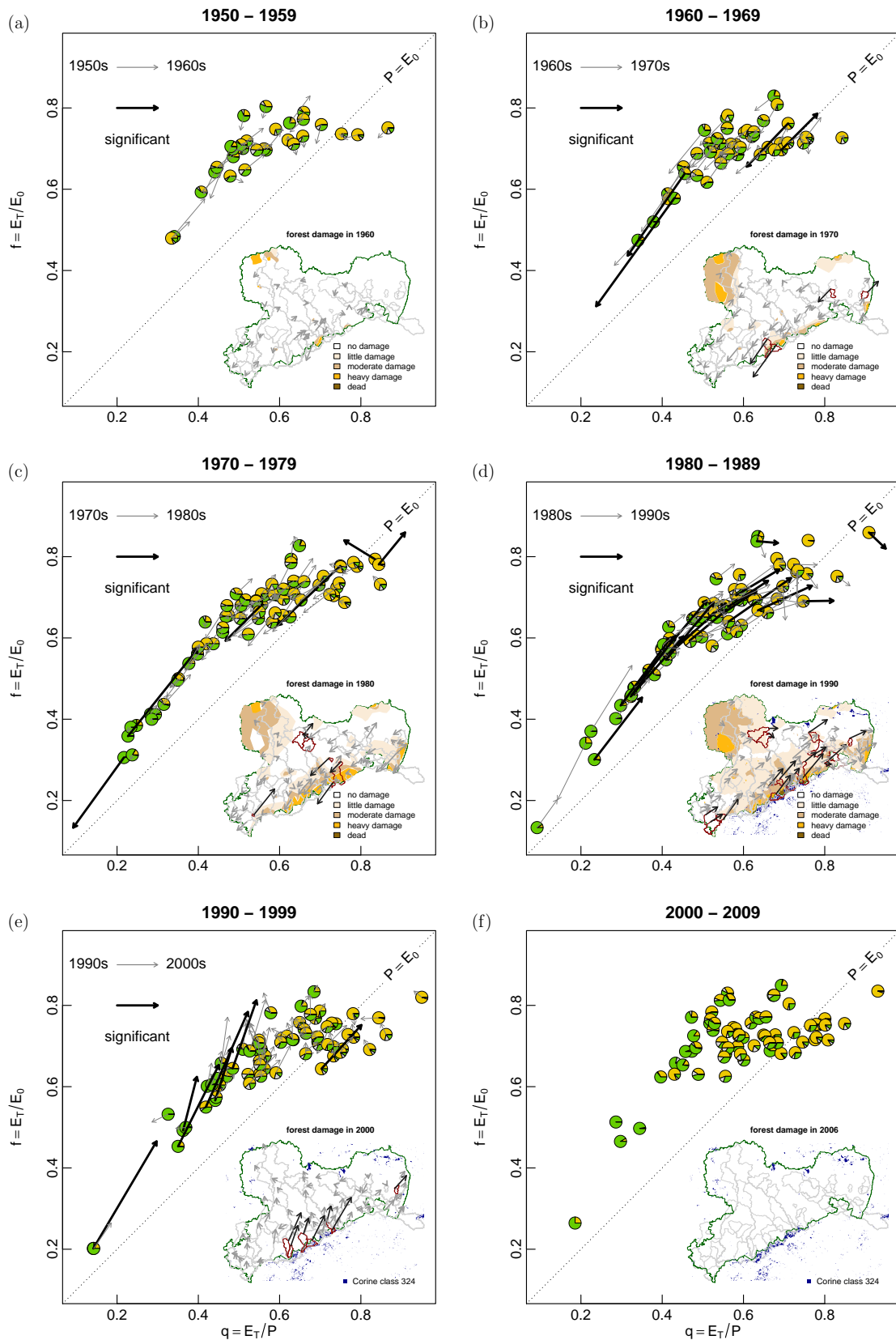


Fig. 7. Annual averages per decade of the water and energy partitioning ratios for each basin analyzed. The arrows denote the change in the $q - f$ ratio in the next decade. Significant changes are marked with bold arrows in the water–energy plot. Land-use of the basins is indicated by the colored pie-charts as in Fig. 6. The inlay maps show the location of the river gauges, the spatial extent of forest damages and since 1990 blue pixels show the CORINE transitional forest class.

observed in the 1970s. In most basins the land-surface related anomalies have the same sign as the climatic changes and show increasing dominance at higher altitudes, which is linked to the forest damages.

Combining hydro-climatic separation results with the forest damage data allows for validation of the separation method. To do so we use the grouping of basins according to the damaged forest area per basin introduced with Fig. 5 to check if the forest damage has an effect on the attributed anomalies. Clearly for the land-surface related anomalies, we would expect that the larger the damaged area, the larger the E_T anomaly. In contrast, the climatic change impacts should be independent of the land-surface impacts. The results of this test are shown in Fig. 8. The panels show the largest E_T anomaly per basin grouped by the percentage of the damaged area. The climatic related E_T anomalies show a gentle decrease in the magnitude of the anomaly with increasing forest damage. This effect is however much smaller than the increase of the absolute land-surface related anomalies with forest damage. There is hardly any distinction between basins without detected damages and damaged areas smaller than 2%. Moderately affected basins between 2 and 20% damage show a trend, whereas strongly affected basins show distinctly larger E_T anomalies.

5 Discussion

5.1 Controls on water–energy partitioning

The long-term average partitioning of water and energy in Saxony shows two dominant patterns. First, there is the control by climatic conditions which is best described by the aridity index. This pattern reveals that under more humid conditions the energy limitation results in higher energy partitioning ratios than water partitioning ratios. Towards non-limited conditions (i.e., $P = E_0$) both ratios are also equal. In Saxony, the humidity gradients are mainly driven by topography. We find that the orographically driven precipitation induces a gradient in available water and available energy for E_T . In general, the effects of the gradients in P and E_0 should be predictable with a Budyko type of function.

However, there is a second emergent pattern, which reveals a large variability of water–energy partitioning along a fixed climate aridity index (Fig. 6). Hence both, energy and water partitioning ratios are simultaneously affected. We hypothesize that this pattern is linked to land-surface related conditions, which effect E_T , but also correlate with altitude. A persistent control is the water storage capacity which is also linked to topography and the presence of aquifers (we used the lagged cross correlation of annual precipitation and runoff as proxy). This control shows a positive correlation to E_T (Table 2) as it determines the availability of water under dry conditions. This finding is in line with Troch et al. (2013) who relate deviations from the Budyko curve to the

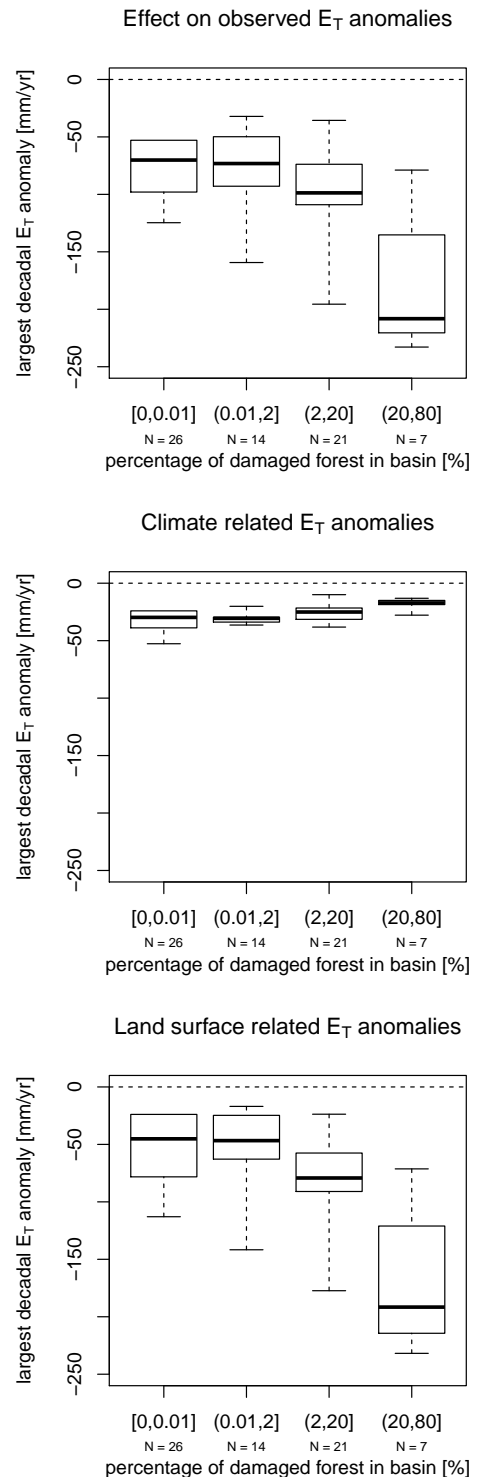


Fig. 8. Largest decadal $P - Q$ anomalies with respect to the last decade (2000–2009) as function of the percentage of damaged forest (Corine 1990, class 324, transitional scrub forest class) in all catchments. (a) Observed anomalies, (b) attributed aridity index change impacts, (c) attributed land-surface change impacts. For all panels the same axes are used.

timescale of a perched aquifer. Another land-surface control is vegetation, which we assessed by land cover classification, just separating into agricultural and forested basins. The type of land-use is naturally correlated to climate and water–energy partitioning, resulting in a negative correlation with forest cover, which is again well correlated with altitude and thus climate aridity. The rather high correlations of land-surface properties to climate reveals strong interactions between climate, soils and vegetation. This equilibrium state may explain the predictive power of the Budyko curve (Gentine et al., 2012).

An intriguing finding of our study, however, is that even on the long term two sets of basins substantially deviate from the Budyko curve. These are low altitude agriculturally dominated basins which are well above the Budyko curve, whereas a set of forest dominated basins exhibit rather small E_T/P and E_T/E_0 ratios. A few agricultural basins show larger decadal dynamics in water–energy partitioning, especially in the 1960s to 1990s. Although some change may be attributed to land management changes towards industrialization of agriculture (Eckart and Wollkopf, 1994; Baessler and Klotz, 2006), the patterns, however, are not very consistent and no detailed data on land management changes was available for this study to identify potential causes. In this study, we focussed on the causes of the low water–energy partitioning ratios of some of the forested basins. The forest damage data revealed that the decadal changes in the water–energy partitioning are due to the forest decline, which explains why these basins are well below the Budyko curve. In the following, we discuss the role of non-stationary changes detected in the water–energy partitioning of these basins.

5.2 The role of environmental pollution on regional scale E_T

Although we discussed the impacts of climate and land-surface change separately, there is some evidence that both have been caused by heavy air pollution throughout central Europe. The aerosol emissions of the coal power stations have led to decreases in surface solar radiation also known as the “global dimming” (Wild et al., 2005), peaking in the 1980s (Ruckstuhl et al., 2008; Philipona et al., 2009). This has had a direct effect on the evaporative demand, which caused a significant reduction in potential evapotranspiration during that time (Fig. 4).

The indirect effects of the air pollution have been more localized due to topographical and meteorological factors favoring an inversion (Pfanzen et al., 1994). An inversion typically leads to frequent foggy conditions, particularly in the mountain ridges (Flemming, 1964). Due to the air pollution the aerosol load in the fog reached very high concentrations (Schulze, 1989; Zimmermann and Zimmermann, 2002). The deposition of the aerosols led to an accumulation of sulphurous acid and other pollutants in the soils (Pfanzen et al., 1994; Zimmermann et al., 2003). This effect was especially

dominant in coniferous forests, which tend to comb out fog due to their large capacity for water interception (Lange et al., 2003). Over time the acidified soils led to changes in the nutrient compositions with reduced magnesium and calcium cations in the soil solution (Schulze, 1989). This resulted in severe tree crown damages, reduced stand productivities and higher vulnerability for other environmental stress factors (Sterba, 1996; Wimmer et al., 2002). Evaporation from interception as well as transpiration must have been drastically reduced by the affected trees, thus affecting both of the processes dominant in shaping total evaporation. The importance for basin scale evapotranspiration is evident from Fig. 5, as well as the decadal water–energy partitioning plots in Fig. 7. The decadal changes highlighted in Fig. 7 show that many higher altitude, forested basins moved along relatively constant aridity lines. These changes are attributed to land-surface change, but the timing of these changes is not synchronized across all catchments. A possible explanation is that the timing of the dominant hydrological effects of the forest damage can differ strongly due to the actual damage and forest management actions such as clear cutting of damaged stands.

The phenomena of the *Waldsterben* appeared on the political agenda in the 1980s and resulted in a common call for reducing power plant emissions. Additionally, the transition from the 1980s to the 1990s marks a period of drastic political, socio-economic changes in the former East Germany and eastern Europe. The industrial breakdown especially accelerated the improvement of environmental conditions and significantly reduced aerosol emissions (Matschullat et al., 2000; Zimmermann et al., 2003). The reduced aerosol emissions quickly increased surface solar radiation, temperatures (Philipona et al., 2009) and, as evident from Fig. 5, also E_T across all basins reaching among the largest values of the study period.

Interestingly, the catchments with damaged forests also show stronger increases in E_T (Fig. 5) consistent over all catchments along the Ore Mountains (see Fig. 7d). This quick and consistent recovery of E_T highlights the importance of understorey and young stands taking over key roles of water and energy partitioning. This fast recovery of E_T might also explain the sign differences of significant water–energy trajectories before 1990 and thus the difficulty in assessing the timing of hydrological impacts of vegetation changes. Together with relatively poor observations describing relevant hydrological land-surface characteristics, this difficulty reduces the predictive power for single basin E_T dynamics from forest damage data alone.

5.3 Potentials and limitations

The methodological contribution of this paper is to provide a framework to classify and separate climatic and land-surface change impacts from observed hydro-climatic changes. The challenge in this problem is that these impacts

may occur simultaneously, but act on different processes and thus scales, including internal responses to these external forcings. The proposed framework, based on mass and energy conservation, may be regarded as the simplest possible first order approach. The separation requires a few strong assumptions, which makes this a transparent and attractive approach for research and practitioners.

The method can be used to identify non-stationary changes in the average water–energy partitioning and to quantify the contributions of the most general impacts (Renner and Bernhofer, 2012). It is, however, important to note that due to the strict definition of climatic change impacts, and the more open definition of land-surface change impacts it is not possible to directly trace the respective process causing the observed change. To identify the role of sub-scale processes, process-based models are required. As these models generally require more input data, they additionally suffer from model parameter and model structure uncertainties (Seibert and McDonnell, 2010). Hence, these more detailed analyses should be approached in a top-down manner (Klemeš, 1983), starting with a simple first order approach as illustrated here.

The proposed method is prone to input data uncertainties, especially precipitation, potential evapotranspiration and runoff data. However, if we assume that random errors average out over longer periods as used here, these uncertainties may diminish. We also tested the influence of systematic uncertainties, such as precipitation bias correction, station network changes, the estimation of potential evapotranspiration, or the uncertainty of deriving spatial basin scale meteorological input data. All of these play a role but resulted in shifting the whole data set rather than changing its shape within the water–energy partitioning plots.

In this analysis, the uncertainty of land-surface related changes was dominant. This is most apparent in Fig. 8c where we analyze the effect of forest cover damage on the land-surface related E_T anomalies. First, there is a large variability across basins, but also note that the land-surface related anomalies are significantly below zero also in basins where no forest-damage has been detected. Apparently, the land-surface related anomalies are on the order of the climate related impacts, which may highlight the uncertainty range of the approach. Yet, it is not clear if the dominant uncertainty arises from the separation method, other land-surface related changes, the input data, or changes in water storage at the chosen averaging periods. However, we argue that the consistence of negative land-surface related anomalies over the study area may rule out the latter two. Apparently, there is a background signal of increasing E_T in all catchments which is attributed to land-surface changes. Similar increases in E_T have been found in the US by Walter et al. (2004) and Renner and Bernhofer (2012). This could indeed be land cover induced changes, for example increasing vegetation growth (McMahon et al., 2010), or increasing human water use for food and energy production (Destouni et al., 2013). But also changes in meteorological variables

not covered in the long-term annual average aridity index may have induced this signal. Hence, the identification of the causes of the recent land-surface attributed increases in E_T should be addressed in further research.

Despite these limitations and the simplicity of the approach, we have been able to show that the timing and spatial extent of forest damage can be linked to distinct land-surface related changes of basin scale E_T . Whereas the anomalies attributed to changes in climate aridity are almost independent from the magnitude of forest damage. This validates the usefulness of the separation framework for the assessment of hydro-climatic changes on decadal timescales.

6 Conclusions

Plotting the ratio of energy partitioning E_T/E_0 vs. the water partitioning ratio E_T/P is a very useful tool to analyze annual average evapotranspiration. This diagram allows for the investigation of the interplay of the water and energy balance and the tight coupling of both through E_T . The diagram can also help to differentiate between climatic and land-surface controls on E_T . Both controls result in qualitatively different patterns of water–energy partitioning. In particular, climatic changes, defined as changes in the aridity index, result in a shift in the diagram which is perpendicular to changes resulting from land-surface changes. This allows a geometrical separation and quantification of climatic and land-surface impacts on E_T .

Testing this approach with data of the well-observed region of Saxony reveals some general insights on how and why this simple approach is successful. First, it is known that vegetation is adapting to climatic conditions and thus reduces the influence of other land-surface conditions such as soils and topography on water–energy partitioning. Hence, long-term annual average E_T can indeed be predicted by the Budyko curve which only requires data on precipitation and evaporative demand. Second, the prevailing climate also determines the hydrological sensitivity to climatic or land-surface changes. Plotting the Budyko curve or decadal average data in water–energy diagrams reveals that adaptation to changes in P or E_0 result in opposing effects on water and energy partitioning. A trend towards a more humid climate will thus reduce the water partitioning ratio (E_T/P), while the energy partitioning ratio (E_T/E_0) will increase. More dry conditions will have opposing effects. This finding is evident from the data of non-disturbed basins in Saxony. This is highly relevant for, for example, water resources management as it determines the amount of available water under changes in precipitation and/or potential evapotranspiration. Third, we detected significant impacts of land-surface changes with the proposed approach. This land-surface change is confirmed by ground based and remote sensing based observations of forest damages in these basins. From these results we conclude that anthropogenic

impacts such as environmental pollution adversely affecting vegetation functioning will lead to declines in E_T (here in the order of 200 mm yr^{-1} or 38%) and thus produce more runoff. The long-term observations also reveal that E_T can recover within the order of decades, although eco-physiological states are far from being recovered yet.

This approach can identify general drivers of change in landscape hydrology solely by using long-term observations of catchment runoff, precipitation and potential evapotranspiration. Since the method is general, it can be transferred to other regions and other climate conditions. The relatively low data demand allows first order impact assessment of past climate and land surfaces as well as estimates on future climate impacts on hydrology, without the need of numerical modeling.

Finally, we have to note that the simplicity of the approach does not allow to attribute certain changes to a more specific process or cause. An intriguing example is that we found that E_T consistently increased in the last two decades (1990–2009). According to the methods definitions, this increase is attributed to a land-surface change. Hence, all basins moved closer to the water and energy limits of evapotranspiration. Although this effect is smaller than the land-surface changes induced by the forest decline, it is of similar magnitude than increases in E_T caused by changes in P or E_0 . While this points to the limits of the proposed approach, it also highlights the potential role of other climatic variables to explain this increase in catchment scale E_T . This should be addressed in future research.

Supplementary material related to this article is available online at <http://www.hydrol-earth-syst-sci.net/18/389/2014/hess-18-389-2014-supplement.pdf>.

Acknowledgement. We acknowledge the Saxon State Office for the Environment, Agriculture and Geology (LfULG) for providing the runoff time series and the German Weather Service (DWD), Czech Hydro-meteorological Service (CHMI) for providing climate data. M. Renner was kindly supported by Helmholtz Impulse and Networking Fund through Helmholtz Interdisciplinary Graduate School for Environmental Research (HIGRADE) (Bissinger and Kolditz, 2008). K. Brust acknowledges support from the German Research Foundation (DFG) grant BE 1721/13. We thank Bethany Shumaker and Lee Miller for checking and improving the language. The valuable comments of three reviewers are gratefully acknowledged.

The service charges for this open access publication have been covered by the Max Planck Society.

Edited by: S. Archfield

References

- Allen, R., Smith, M., Pereira, L., and Perrier, A.: An update for the calculation of reference evapotranspiration, *ICID Bull.*, 43, 35–92, 1994.
- Arnell, N.: *Hydrology and Global Environmental Change*, Pearson Education, Harlow, 2002.
- Arora, V.: The use of the aridity index to assess climate change effect on annual runoff, *J. Hydrol.*, 265, 164–177, 2002.
- Baessler, C. and Klotz, S.: Effects of changes in agricultural land-use on landscape structure and arable weed vegetation over the last 50 years, *Agriculture, Ecosyst. Environ.*, 115, 43–50, doi:10.1016/j.agee.2005.12.007, 2006.
- Bernhofer, C., Goldberg, V., Franke, J., Häntzschel, J., Harmansa, S., Pluntke, T., Geidel, K., Surke, M., Prasse, H., Freydank, E., Hänsel, S., Mellentin, U., and Küchler, W.: *Klimamonographie für Sachsen (KLIMOSA) – Untersuchung und Visualisierung der Raum- und Zeitstruktur diagnostischer Zeitreihen der Klimatelemente unter besonderer Berücksichtigung der Witterungsextreme und der Wetterlagen, Sachsen im Klimawandel, Eine Analyse, Sächsisches Staats-Ministerium für Umwelt und Landwirtschaft (Hrsg.)*, Dresden, p. 211, 2008.
- Bissinger, V. and Kolditz, O.: Helmholtz Interdisciplinary Graduate School for Environmental Research (HIGRADE), *GAIA – Ecol. Perspect. Sci. Soc.*, 17, 71–73, 2008.
- Blöschl, G. and Montanari, A.: Climate change impacts' throwing the dice?, *Hydrol. Process.*, 24, 374–381, doi:10.1002/hyp.7574, 2010.
- Bossard, M., Feranec, J., and Otahel, J.: *CORINE land cover technical guide: Addendum 2000*, European Environment Agency Copenhagen, Copenhagen, Denmark, 2000.
- Budyko, M.: *Evaporation under natural conditions*, Gidrometeorizdat, Leningrad, English translation by IPST, Jerusalem, 1948.
- Budyko, M.: *Climate and life*, Academic press, New York, USA, 1974.
- Choudhury, B.: Evaluation of an empirical equation for annual evaporation using field observations and results from a biophysical model, *J. Hydrol.*, 216, 99–110, 1999.
- Dale, V. H.: The relationship between land-use change and climate change, *Ecological applications*, 7, 753–769, 1997.
- Destouni, G., Jaramillo, F., and Prieto, C.: Hydroclimatic shifts driven by human water use for food and energy production, *Nat. Clim. Change*, 3, 213–217, doi:10.1038/nclimate1719, 2013.
- Donohue, R. J., Roderick, M. L., and McVicar, T. R.: On the importance of including vegetation dynamics in Budyko's hydrological model, *Hydrol. Earth Syst. Sci.*, 11, 983–995, doi:10.5194/hess-11-983-2007, 2007.
- Donohue, R. J., McVicar, T. R., and Roderick, M. L.: Assessing the ability of potential evaporation formulations to capture the dynamics in evaporative demand within a changing climate, *J. Hydrol.*, 386, 186–197, doi:10.1016/j.jhydrol.2010.03.020, 2010.
- Dooge, J.: Sensitivity of runoff to climate change: A Hortonian approach, *B. Am. Meteorol. Soc. USA*, 73, 2013–2024, 1992.
- Eckart, K. and Wollkopf, H.-F.: *Landwirtschaft in Deutschland: Veränderungen der regionalen Agrarstruktur in Deutschland zwischen 1960 und 1992*, Institut für Landerkunde, <http://www.opengrey.eu/item/display/10068/216447> (last access: 27 June 2013), 1994.

- Flemming, G.: Meteorologische Überlegungen zum forstlichen Rauchsadensgebiet am Erzgebirgskamm, *Wiss. Z. Techn. Univers. Dresden*, 13, 1531–1538, 1964.
- Forstprojektion: Aufnahme von Schadstufen bei Rauchsäden Betriebsregelungsanweisung – BRA IV/320, VEB Forstprojektion, 1970.
- Fu, B.: On the calculation of the evaporation from land surface, *Sci. Atmos. Sin.*, 5, 23–31, 1981.
- Gentine, P., D'Odorico, P., Lintner, B. R., Sivandran, G., and Salvucci, G.: Interdependence of climate, soil, and vegetation as constrained by the Budyko curve, *Geophys. Res. Lett.*, 39, L19404, doi:10.1029/2012GL053492, 2012.
- Grünwald, U.: Water resources management in river catchments influenced by lignite mining, *Ecol. Eng.*, 17, 143–152, 2001.
- Hiemstra, P., Pebesma, E., Twenhöfel, C., and Heuvelink, G.: Real-time automatic interpolation of ambient gamma dose rates from the dutch radioactivity monitoring network, *Comput. Geosci.*, 35, 1711–1721, 2009.
- Istanbulluoglu, E., Wang, T., Wright, O. M., and Lenters, J. D.: Interpretation of hydrologic trends from a water balance perspective: The role of groundwater storage in the Budyko hypothesis, *Water Resour. Res.*, 48, W00H16, doi:10.1029/2010WR010100, 2012.
- Jaramillo, F., Prieto, C., Lyon, S. W., and Destouni, G.: Multimethod assessment of evapotranspiration shifts due to non-irrigated agricultural development in Sweden, *J. Hydrol.*, 484, 55–62, doi:10.1016/j.jhydrol.2013.01.010, 2013.
- Jarvis, A., Reuter, H., Nelson, E., and Guevara, E.: Hole-filled seamless SRTM data version 4, International Center for Tropical Agriculture (CIAT), available at: <http://srtm.csi.cgiar.org> (last access: 27 June 2013), 2008.
- Jones, J.: Hydrologic responses to climate change: considering geographic context and alternative hypotheses, *Hydrol. Process.*, 25, 1996–2000, 2011.
- Klemeš, V.: Conceptualization and scale in hydrology, *J. Hydrol.*, 65, 1–23, 1983.
- Lange, C. A., Matschullat, J., Zimmermann, F., Sterzik, G., and Wienhaus, O.: Fog frequency and chemical composition of fog water – a relevant contribution to atmospheric deposition in the eastern Erzgebirge, Germany, *Atmos. Environ.*, 37, 3731–3739, 2003.
- Matschullat, J., Maenhaut, W., Zimmermann, F., and Fiebig, J.: Aerosol and bulk deposition trends in the 1990's, Eastern Erzgebirge, Central Europe, *Atmos. Environ.*, 34, 3213–3221, 2000.
- McMahon, S. M., Parker, G. G., and Miller, D. R.: Evidence for a recent increase in forest growth, *P. Natl. Acad. Sci.*, 107, 3611–3615, doi:10.1073/pnas.0912376107, 2010.
- Merz, R., Parajka, J., and Bloeschl, G.: Time stability of catchment model parameters: Implications for climate impact analyses, *Water Resour. Res.*, 47, W02531, doi:10.1029/2010WR009505, 2011.
- Mezentsev, V.: More on the calculation of average total evaporation, *Meteorol. Gidrol.*, 5, 24–26, 1955.
- Milliman, J., Farnsworth, K., Jones, P., Xu, K., and Smith, L.: Climatic and anthropogenic factors affecting river discharge to the global ocean, 1951–2000, *Global Planet. Change*, 62, 187–194, 2008.
- Milly, P. and Dunne, K.: Trends in evaporation and surface cooling in the Mississippi River basin, *Geophys. Res. Lett.*, 28, 1219–1222, doi:10.1029/2000GL012321, 2001.
- Milne, B., Gupta, V., and Restrepo, C.: A scale invariant coupling of plants, water, energy, and terrain, *Ecoscience*, 9, 191–199, 2002.
- Ol'Dekop, E.: On evaporation from the surface of river basins, *T. Meteorol. Observ. Univ. Tartu*, 4, 200 pp., 1911.
- Pfanz, H., Vollrath, B., Lomsky, B., Oppmann, B., Hynek, V., Beyschlag, W., Bilger, W., White, M., and Materna, J.: Life expectancy of spruce needles under extremely high air pollution stress: performance of trees in the Ore Mountains, *Trees-Struct. Funct.*, 8, 213–222, 1994.
- Philipona, R., Behrens, K., and Ruckstuhl, C.: How declining aerosols and rising greenhouse gases forced rapid warming in Europe since the 1980s, *Geophys. Res. Lett.*, 36, L02806, doi:10.1029/2008GL036350, 2009.
- Pielke, R. A.: Land Use and Climate Change, *Science*, 310, 1625–1626, doi:10.1126/science.1120529, 2005.
- Pike, J.: The estimation of annual run-off from meteorological data in a tropical climate, *J. Hydrol.*, 2, 116–123, 1964.
- Renner, M. and Bernhofer, C.: Long term variability of the annual hydrological regime and sensitivity to temperature phase shifts in Saxony/Germany, *Hydrol. Earth Syst. Sci.*, 15, 1819–1833, doi:10.5194/hess-15-1819-2011, 2011.
- Renner, M. and Bernhofer, C.: Applying simple water-energy balance frameworks to predict the climate sensitivity of streamflow over the continental United States, *Hydrol. Earth Syst. Sci.*, 16, 2531–2546, doi:10.5194/hess-16-2531-2012, 2012.
- Renner, M., Seppelt, R., and Bernhofer, C.: Evaluation of water-energy balance frameworks to predict the sensitivity of streamflow to climate change, *Hydrol. Earth Syst. Sci.*, 16, 1419–1433, doi:10.5194/hess-16-1419-2012, 2012.
- Richter, D.: Ergebnisse methodischer Untersuchungen zur Korrektur des systematischen Messfehlers des Hellmann-Niederschlagsmessers, *Deutscher Wetterdienst*, 1995.
- Roderick, M. and Farquhar, G.: A simple framework for relating variations in runoff to variations in climatic conditions and catchment properties, *Water Resour. Res.*, 47, W00G07, doi:10.1029/2010WR009826, 2011.
- Ruckstuhl, C., Philipona, R., Behrens, K., Collaud Coen, M., Dürr, B., Heimo, A., Mätzler, C., Nyeki, S., Ohmura, A., Vuilleumier, L., Weller, M., Wehrli, C., and Zelenka, A.: Aerosol and cloud effects on solar brightening and the recent rapid warming, *Geophys. Res. Lett.*, 35, L12708, doi:10.1029/2008GL034228, 2008.
- Schreiber, P.: Über die Beziehungen zwischen dem Niederschlag und der Wasserführung der Flüsse in Mitteleuropa, *Z. Meteorol.*, 21, 441–452, 1904.
- Schulze, E.-D.: Air Pollution and Forest Decline in a Spruce (Picea abies) Forest, *Science*, 244, 776–783, doi:10.1126/science.244.4906.776, 1989.
- Seibert, J. and McDonnell, J. J.: Land-cover impacts on streamflow: a change-detection modelling approach that incorporates parameter uncertainty, *Hydrolog. Sci. J.*, 55, 316–332, doi:10.1080/02626661003683264, 2010.
- SMUL: in: *Waldzustandsbericht, Sachsenforst, Pirna*, 2006.
- Šrámek, V., Slodičák, M., Lomský, B., Balcar, V., Kulhavý, J., Hadaš, P., Pulkráb, K., Šišák, L., Pěnička, L., and Sloup, M.: The Ore Mountains: Will successive recovery of forests from lethal disease be successful, *Mt. Res. Dev.*, 28, 216–221, 2008.

- StaLa: Statistischer Bericht, Flächenerhebung nach Art der tatsächlichen Nutzung im Freistaat Sachsen, 2011, Tech. rep., Statistisches Landesamt des Freistaates Sachsen, Kamenz, http://www.statistik.sachsen.de/download/100_Berichte-A/A_V_1_j11_SN.pdf (last access: 27 June 2013), 2012.
- Sterba, H.: Forest Decline and Growth Trends in Central Europe – a Review, in: Growth Trends in European Forests, edited by: Spiecker, H., Mielikäinen, K., Köhl, M., and Skovsgaard, J. P., Springer, Berlin, Heidelberg, 149–165, 1996.
- Theil, H.: A rank-invariant method of linear and polynomial regression analysis (Parts 1–3), *Nederlandse Akademie Wetenschappen Series A*, 53, 386–392, 1950.
- Todorov, V. and Filzmoser, P.: An Object-Oriented Framework for Robust Multivariate Analysis, *J. Stat. Softw.*, 32, 1–47, 2009.
- Tomer, M. and Schilling, K.: A simple approach to distinguish land-use and climate-change effects on watershed hydrology, *J. Hydrol.*, 376, 24–33, doi:10.1016/j.jhydrol.2009.07.029, 2009.
- Troch, P. A., Carrillo, G., Sivapalan, M., Wagener, T., and Sawicz, K.: Climate-vegetation-soil interactions and long-term hydrologic partitioning: signatures of catchment co-evolution, *Hydrol. Earth Syst. Sci.*, 17, 2209–2217, doi:10.5194/hess-17-2209-2013, 2013.
- Walter, M., Wilks, D., Parlange, J., and Schneider, R.: Increasing Evapotranspiration from the Conterminous United States, *J. Hydrometeorol.*, 5, 405–408, 2004.
- Wang, D. and Hejazi, M.: Quantifying the relative contribution of the climate and direct human impacts on mean annual streamflow in the contiguous United States, *Water Resour. Res.*, 47, W00J12, doi:10.1029/2010WR010283, 2011.
- Wild, M., Gilgen, H., Roesch, A., Ohmura, A., Long, C. N., Dutton, E. G., Forgan, B., Kallis, A., Russak, V., and Tsvetkov, A.: From Dimming to Brightening: Decadal Changes in Solar Radiation at Earth's Surface, *Science*, 308, 847–850, doi:10.1126/science.1103215, 2005.
- Wimmer, R., Hinterstoisser, B., Stanzl-Tschegg, S., Grabner, M., Wallner, G., Halbwegs, G., Schär, E., and Wagenführ, R.: Anatomical, Chemical and Mechanical Trends in Norway Spruce (*Picea abies* [L.] Karst.), Tree Rings as Indicators of Environmental Stresses, in: Particular SO₂-pollution, SO₂-Pollution and Forest Decline in the Ore Mountains, edited by: Lomsky, B., Materna, J., and Pfan, H., Jiloviště-Strnady, Forestry and Game Management Research Institute, Vůlhm, 239–260, 2002.
- Yang, H., Yang, D., Lei, Z., and Sun, F.: New analytical derivation of the mean annual water-energy balance equation, *Water Resour. Res.*, 44, W03410, doi:10.1029/2007WR006135, 2008.
- Zimmermann, F., Lux, H., Maenhaut, W., Matschullat, J., Plessow, K., Reuter, F., and Wienhaus, O.: A review of air pollution and atmospheric deposition dynamics in southern Saxony, Germany, Central Europe, *Atmos. Environ.*, 37, 671–691, doi:10.1016/S1352-2310(02)00829-4, 2003.
- Zimmermann, L. and Zimmermann, F.: Fog deposition to Norway Spruce stands at high-elevation sites in the Eastern Erzgebirge (Germany), *J. Hydrol.*, 256, 166–175, doi:10.1016/S0022-1694(01)00532-7, 2002.
- Zirlewagen, D.: Ableitung einer Schadzonierung für die Wälder Sachsens durch Anwendung statistischer Methoden, Abschlussbericht zum Forschungsvorhaben, Graupa, 2004.